

See discussions, stats, and author profiles for this publication at: <https://www.researchgate.net/publication/51856456>

First-Principles Assessment of H₂S and H₂O Reaction Mechanisms and the Subsequent Hydrogen Absorption on CeO₂(111) Surface.

ARTICLE in THE JOURNAL OF PHYSICAL CHEMISTRY A · DECEMBER 2011

Impact Factor: 2.69 · DOI: 10.1021/jp205573v · Source: PubMed

CITATIONS

40

READS

3

2 AUTHORS:



Dario Marocchelli

Massachusetts Institute of Technology

46 PUBLICATIONS 634 CITATIONS

[SEE PROFILE](#)



Bilge Yildiz

Massachusetts Institute of Technology

130 PUBLICATIONS 1,683 CITATIONS

[SEE PROFILE](#)

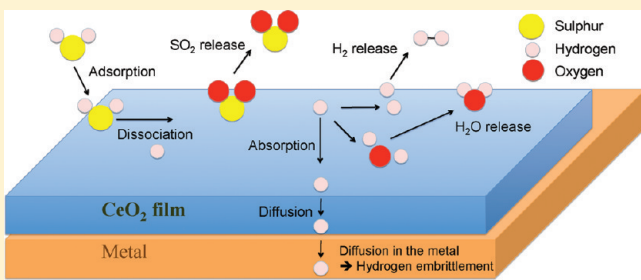
First-Principles Assessment of H₂S and H₂O Reaction Mechanisms and the Subsequent Hydrogen Absorption on the CeO₂(111) Surface

Dario Marrocchelli[†] and Bilge Yildiz*

Laboratory for Electrochemical Interfaces, Department of Nuclear Science and Engineering, Massachusetts Institute of Technology, 77 Massachusetts Avenue, Cambridge, Massachusetts 02139, United States

Supporting Information

ABSTRACT: The main goal of this study is to assess the resistance of ceria against hydrogen penetration into its bulk, in the context of its application as a protective surface coating against hydrogen embrittlement in metals. We evaluate the reaction mechanisms between the H₂S and H₂O molecules and the CeO₂(111) surface and their kinetic descriptors, using first principles based calculations in the density functional theory framework. Our approach is validated by performing an extensive comparison with the available experimental data. We predict that hydrogen penetration into CeO₂(111) is a surface-absorption-limited process with a high-energy barrier (1.67 eV) and endothermicity (1.50 eV), followed by a significantly lower bulk dissolution energy and diffusion barrier (0.67 and 0.52 eV, respectively). We find that the presence of surface vacancies and higher coverages affects significantly the energetics of H₂S/H₂O adsorption, dissociation, and hydrogen subsurface absorption, facilitating most of these processes and degrading the protectiveness of ceria against hydrogen penetration. The reasons behind these effects are discussed. Overall we expect ceria to hinder the hydrogen incorporation significantly due to the effectively large energy barrier against subsurface absorption, provided vacancy formation is suppressed.



INTRODUCTION

CeO₂, cerium dioxide or ceria, is a technologically important material which has found applications in catalysis,¹ Solid Oxide Fuel Cells (SOFCs),^{2,3} and thermochemical water splitting.⁴ Ceria plays an important role in catalysis thanks to its oxygen storage capability due to the ready oxidation state change from Ce⁴⁺ to Ce³⁺ upon reduction and the reverse upon oxidation.¹ These properties are made use of in Three-Way Catalysts (TWC),¹ where the stored oxygen aids in the oxidation of CO to CO₂ under reducing conditions. Under fuel-lean conditions, the reduction of NO to N₂ is assisted by the uptake of oxygen by ceria.⁵ Doping ceria with aliovalent cations, such as Gd, Y, or Sm, leads to high ionic conductivity in the intermediate temperature range (500–800 °C), thus raising the prospects of ceria-based electrolytes for application in SOFCs.^{3,6,7} Recently this material was also suggested as a high-temperature sulfur sorbent, which can be used to protect nickel-based anode materials in SOFCs from sulfur poisoning.⁸

Another potential application for this material is its use as a protective oxide coating on metals in corrosive environments to prevent them from hydrogen embrittlement (HE). Hydrogen embrittlement is a process that is triggered with the adsorption and dissociation of H-containing species, such as H₂, H₂O, and H₂S, on the surface of a metal.^{9–11} The dissociated protons or hydrogen atoms subsequently get absorbed into the subsurface and penetrate into the bulk of the material. Once in the bulk, through various mechanisms, most prominently via

hydrogen-induced decohesion or hydrogen-enhanced localized plasticity,¹² the presence of hydrogen severely degrades the ductility and fracture toughness of the metals. While impacting a wide spectrum of infrastructures, HE is of particular importance in oil production and exploration fields since H₂S and H₂O are present in the drilling fluids, and H₂S, in particular, is thought to be very aggressive to steels and Ni alloys.^{13,14} Drilling environments contain up to several thousand parts per million of H₂S, and their temperatures and pressure are usually 50–200 °C and up to 200 MPa, respectively.^{15,16} Coating a thin oxide film onto the alloys could hinder some of the above-mentioned processes and therefore protect materials from HE. A limited amount of work^{17,18} has been done so far to study the performance of oxide coatings for this purpose. Since undoped ceria was found to be a poor proton conductor,¹⁹ provided its grains are micrometer-sized, it is selected here as a model system to investigate the hydrogen release and hydrogen absorption characteristics of its near-surface region. This paper can also be seen as a first computational assessment of the protectiveness of this material against HE.

Clearly, in all the above-mentioned applications, CeO₂ comes in contact with either H₂O or H₂S or mixtures of these two. It is therefore of great importance to obtain an atomic-scale

Received: June 14, 2011

Revised: December 5, 2011

Published: December 06, 2011

understanding of the interactions between these two species and a ceria surface. Such an understanding could provide insights into how to improve the microchemical and microstructural aspects of ceria used in various applications. For this reason, in this paper, we use first principles-based calculations using the Density Functional Theory (DFT) framework to assess the key reactions and parameters that govern the H₂S/H₂O surface reaction mechanisms and kinetics on CeO₂.

Ceria has been the subject of several experimental^{18–30} and theoretical^{31–48} studies. Its surface atomic structure, for instance, has been studied by Esch et al. by a combination of high-resolution Scanning Tunneling Microscopy (STM) and DFT+U calculations.²⁴ In this study, Esch et al. found that vacancies cluster (both in linear arrays and in trimers) on the CeO₂ surface and that these clusters exclusively expose the reduced cerium ions, Ce³⁺, and include subsurface vacancies. Subsequent studies²⁶ have focused on these subsurface vacancies and found evidence to their local ordering, which suggests the existence of a delicate balance between subtle interactions among adjacent subsurface oxygen vacancy structures. In another study, Gritschneider et al. succeeded to visualize the atomic structure of CeO₂(111), its defects, and the adsorption of water and oxygen molecules.²⁵ They showed that water readily adsorbs on the surface and forms hydroxide if oxygen vacancies are present, while both the stoichiometric and defective surfaces are rather inert against exposure to molecular oxygen.

To date, however, the interaction of ceria surfaces with H₂S has been less studied compared to H₂O. Mullins et al.²⁷ are, to the authors' knowledge, the only ones to have systematically characterized the interaction between H₂S and the CeO₂(111) surface. In their work they grow *in situ* CeO₂(111) thin films on a Ru(0001) substrate and characterize these by means of X-ray Photoemission Spectroscopy (XPS) and Temperature-Programmed Desorption (TPD). They find that H₂S weakly chemisorbs on fully oxidized ceria, desorbing near 155 K. As ceria is reduced, the desorption temperature for the chemisorbed H₂S decreases. This was explained in terms of the higher degree of dissociative adsorption on reduced ceria. When more strongly bound species, such as HS⁻, OH⁻, and S²⁻, are produced, these crowd the surface and weaken the Ce–H₂S bond. It was also suggested that hydrogen from H₂S reacts with the surface oxygens and produces small quantities of water which is observed to desorb between 200 and 450 K, though the authors discuss the possibility that this is an experimental artifact. Water desorption is enhanced when ceria is reduced and a strong desorption peak is observed near 580 K. When ceria is reduced up to 70% in its near-surface region, corresponding to a CeO_{1.65} stoichiometry, water formation is suppressed, and H₂ desorbs near 580 K. We note, however, that when ceria is so highly reduced it is not expected to be in the fluorite structure anymore.⁷ Indeed, Mullins et al.⁴⁹ observe that the surface structure of reduced films is consistent with the bixbyite crystal structure. For all the stoichiometries studied and throughout the whole temperature range of Mullins and co-workers' experiments, no SO_x species was observed to desorb from the surface.²⁷

From a computational point of view, ceria has been studied extensively within the framework of Density Functional Theory.^{32–43,45–47} Unfortunately these studies used different technical details (DFT versus DFT+U), system sizes (from 24 atoms to 240), and various coverages. It is therefore not surprising that some existing results are at odds with each other. The case of water interactions with a CeO₂(111) surface serves as a

good example of the set of contradictory results. Indeed, this problem has been studied by several groups,^{40–42,45} and their adsorption and dissociation energies and adsorption geometries, on both stoichiometric and reduced surfaces, are different from each other in each reported study. The first study in this field was performed by Kumar et al.⁴⁰ who used DFT calculations (without a U correction) to study the adsorption of water on stoichiometric and reduced CeO₂(111) surfaces, with coverages of 0.5 and 1.0 ML. They found that water adsorbs on top of a Ce cation in stoichiometric ceria, with an adsorption energy $E_{ad} = -0.58$ eV. For reduced ceria, they find that the most stable adsorption geometry ($E_{ad} = -0.72$ eV) is when the water molecule adsorbs on top of a Ce cation, with a vacancy in the third layer from the surface, right below the Ce cation. Their calculations were performed on a very small slab (24 atoms), so it was suggested that these results were affected by size effects, especially when studying reduced ceria.⁴¹ On the other hand, Watkins et al. performed both DFT and DFT+U calculations on (2 × √2) stoichiometric and reduced ceria surface⁴¹ and found that water adsorbs on the former with an energy $E_{ad} = -0.35$ eV and on the latter with an energy $E_{ad} = -0.8$ eV. Contrary to the results of Kumar et al., they find that water adsorbs on top of a surface vacancy. The coverage is not specified in their work, but it seems that they consider a single molecule on the simulation cell surface, which, assuming Ce atop to be the only possible adsorption sites, should correspond to a coverage of 0.25 ML. They also studied the dissociation of water on a reduced surface (by performing short ab initio molecular dynamics simulations) and found this process to be very rapid (<50 ps). Fronzi et al.⁴² examined the atomic structure and energetics of various configurations of water adsorption and dissociation (for a coverage of 0.25 ML) on a reduced and stoichiometric (2 × 2) ceria surface. They chose not to use a DFT+U approach and obtained an adsorption energy $E_{ad} = -0.49$ eV for stoichiometric ceria and $E_{ad} = -1.28$ eV for reduced ceria. They find water dissociation on reduced ceria to have an energy barrier of 2.35 eV, in strong disagreement with the previous results from Watkins et al.⁴¹ Finally, a recent DFT+U study by Yang et al. obtained results similar to Watkins et al.,⁴¹ although their adsorption energy for a water molecule on reduced ceria was smaller, $E_{ad} = -0.54$ eV. In conclusion, the current literature on water interactions with ceria is rather contradictory. While the main objective of this paper is to compare the behavior of H₂O and H₂S on CeO₂, in this work we also try to provide an explanation and conciliation to some of the above-mentioned contradictions.

As in the experimental case, H₂S on a ceria surface has been less studied computationally than the H₂O on ceria. Chen et al. have characterized the potential energy profiles for the interaction between a *single* H₂S molecule and the CeO₂(111) surface along the three channels producing H₂, H₂O, and SO₂.³⁸ They found that H₂S adsorption on CeO₂(111) is weak ($E_{ad} = -0.15$ eV) and is followed by dehydrogenation processes, forming surface S²⁻ and OH⁻ species with an exothermicity of 29.9 kcal/mol (1.30 eV). Their calculations show that the SO₂-forming pathway is energetically most favorable, with an exothermicity of -9.1 kcal/mol (-0.40 eV). This is in strong contradiction with the experimental evidence from Mullins et al. who do not observe any formation of SO_x species.²⁷ To date, to the knowledge of the authors, no results from DFT calculations assessing the H₂S interactions with a reduced CeO₂ surface or proton/hydrogen absorption processes have been reported.

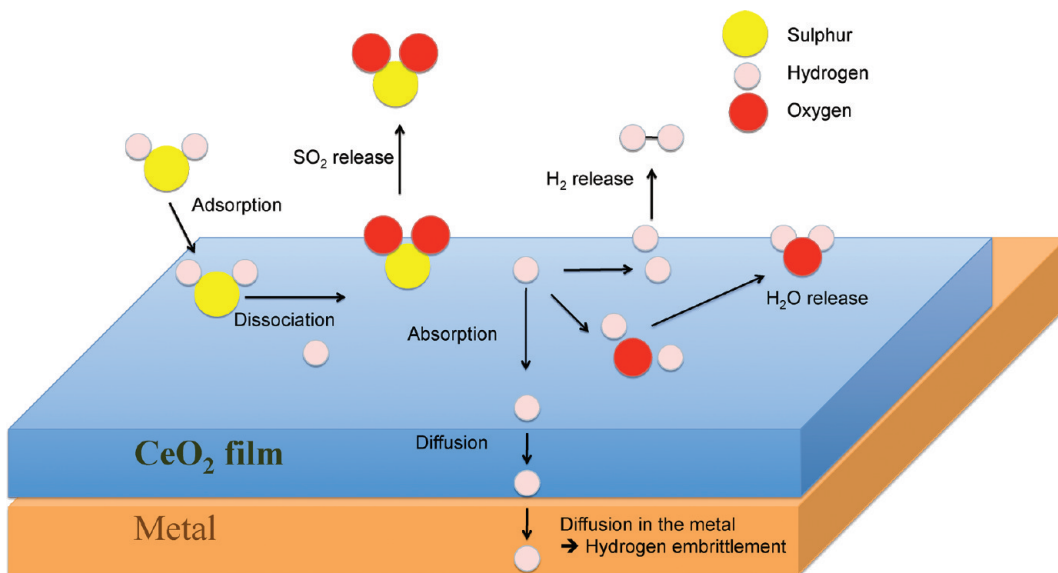


Figure 1. Summary of the studied reactions between a H_2S molecule and a $\text{CeO}_2(111)$ surface.

From the above discussion, it is clear that further work is required to better understand the interaction of H_2S and H_2O molecules on a CeO_2 surface. While some interaction steps have been studied individually, a comparison between H_2S and H_2O is missing. Some of the previous calculations are in disagreement either with each other or with the experimental evidence. Importantly, none of the computational work thus far has evaluated the proton transfer into, and the proton transport in, ceria. While this process is important to consider for the protectiveness of ceria against HE, recently this topic has also attracted great attention in the proton-conducting oxides field.^{29,30} Finally, it is not always clear how these interactions are affected by factors such as oxygen vacancy concentration and/or by the $\text{H}_2\text{S}/\text{H}_2\text{O}$ coverage. In this paper we present a computational study of the H_2S and H_2O interactions with the $\text{CeO}_2(111)$ surface, compare the behavior of these two molecules on the surface, assess the subsequent hydrogen absorption and transport in ceria, and identify the effects that oxygen vacancies and different coverages have on these processes in a systematic way. The rest of the paper first reports the computational methodology, followed by our results. Next a discussion of our findings, including comparisons to available experimental results, is provided. Lastly, the key conclusions of our work are summarized.

■ COMPUTATIONAL METHODOLOGY

We used density functional theory calculations of the equilibrium configurations and static energetics to assess the interactions of H_2S and H_2O with the $\text{CeO}_2(111)$ surface. All the calculations presented in this paper were performed with the Vienna Ab-initio Simulation Package (VASP)^{50,51} with the Projector Augmented Wave (PAW) method. We used the Generalized Gradient Approximation (GGA) with the Perdew–Wang 91 (PW91) exchange-correlation functional and an energy cutoff of 400 eV. Since DFT cannot describe properly the localized nature of the $4f$ electrons and therefore predicts a metallic ground state for reduced ceria, a Hubbard term, with $U = 5$ eV,^{34,35,37} was added. This ensures that an insulating

ground state is obtained for reduced ceria, and the DFT+U method has become the state-of-the-art approach for simulating this material.^{32–35,37} All the calculations were carried out using the Brillouin zone sampled with a $(2 \times 2 \times 1)$ Monkhorst-Pack mesh k -points grid. These settings are in line with those previously used in the literature for $\text{CeO}_2(111)$,^{34,35,38} and convergence tests were performed to make sure that the results are well converged with respect to these parameters.

To study the interactions of the molecules with a surface, the slab method⁵² was used. In this method a finite number of crystal layers in a three-dimensional periodic cell is used to generate two surfaces via the introduction of a vacuum gap perpendicular to the surface. We created a slab exposing the (111) CeO_2 surface, with a $p(2 \times \sqrt{3})$ lateral cell. The slab's surface was $7.6 \text{ \AA} \times 6.6 \text{ \AA} \approx 50 \text{ \AA}^2$, and it was 16 \AA deep, i.e., 15 atomic layers. The vacuum gap was 14 \AA . These dimensions ensured that the energies were well converged. Unless otherwise stated, we placed one molecule on our surface. When we quantify the coverage with respect to the exposed cerium atoms on the surface as adsorption sites, this corresponds to a coverage of 0.25 ML. Adsorption energies, E_{ad} were calculated as

$$E_{\text{ad}} = E[\text{CeO}_2 + \text{adsorbate}] - E[\text{CeO}_2] - E[\text{adsorbate}]$$

where $E[\text{CeO}_2 + \text{adsorbate}]$ is the total energy of a ceria surface with an adsorbed molecule; $E[\text{CeO}_2]$ is the energy of the surface only; and $E[\text{adsorbate}]$ is the energy of a free molecule. The latter was obtained by calculating the energy of the adsorbate molecule in a 15 \AA per side box. The dissociation and absorption energies were calculated from the difference between the energy of the optimized structures of the initial and final states of the reactions. Minimum Energy Paths (MEPs) and the corresponding energy barriers for each reaction studied here (see Figure 1) were obtained by using the climbing image Nudge Elastic Band (NEB) method,⁵³ implemented in VASP. At least three images, though often more, were used for these calculations. The resulting saddle points were confirmed by performing numerical frequency analysis to verify that there exists one and only one imaginary frequency.

Table 1. Elastic Constants (C_{11} , C_{12} , C_{44}), Bulk Modulus (B), and Lattice Parameter (a) for Bulk CeO_2 , Together with the Experimental Values

property	DFT+U	experiments
C_{11} (GPa)	410	386–450 ^{55,56}
C_{12} (GPa)	122	105–124 ^{55,56}
C_{44} (GPa)	80	60–73 ^{55,56}
B (GPa)	218	204–236 ^{55,56}
a (Å)	5.493	5.411 ⁵⁷

Table 2. Unrelaxed and Relaxed Surface Energies for the Three Low Index Surfaces^a

surface type	unrelaxed energy	relaxed energy
(111)	0.68	0.64
(110)	1.63	1.39
(100)	2.39	1.65

^a All values are in units of J/cm².

Validation. DFT+U has been used extensively for the study of both stoichiometric and reduced CeO_2 , and its validity has been assessed thoroughly.^{32–39,42,43,45–47} For this reason, in this work we only tested those properties which are of close interest to the current study. The lattice constant, elastic constants, and bulk modulus for bulk ceria are reported in Table 1, together with the experimental values and with those obtained in previous DFT studies.^{34,35} The surface energies for the (100), (110), and (111) surfaces were then calculated. These are reported in Table 2. The (111) surface is found to be the most stable, in agreement with both the experimental evidence⁵⁴ and previous calculations.^{31,34} A further comparison with experimental data is reported in the Discussion section.

RESULTS

Figure 1 shows all the studied reactions between an H_2S molecule and a $\text{CeO}_2(111)$ surface, as a possible subset of interaction mechanisms between the two. Starting from the left-hand side of the figure, an H_2S molecule first adsorbs on the surface and then dissociates, losing first one hydrogen atom (first dehydrogenation) and then a second one (second dehydrogenation). After this, a series of different processes follow. The sulfur left on the surface reacts with two oxygens and produces a SO_2 molecule on the surface, which is then released from the surface. Alternatively, the hydrogen atoms released onto the surface form a H_2 molecule or react with an oxygen to produce a H_2O molecule. Both molecules are then released into the atmosphere. Finally, the hydrogen atoms or protons are absorbed into the oxide film and diffuse into its bulk. This latter process is the one that compromises the underlying metal for HE. We expect that a thorough characterization of all the possible processes which lead to hydrogen absorption, as demonstrated here, leads to an assessment of the effectiveness of this material as a protective oxide coating on metals against HE.

In this section, we assess all the processes reported in Figure 1 and how these (in particular those involving H_2S) are affected by the presence of oxygen vacancies and different adsorbate (H_2S) coverages. These two factors were found to affect significantly the adsorption and dissociation of H_2O on ceria^{40–42} and on other

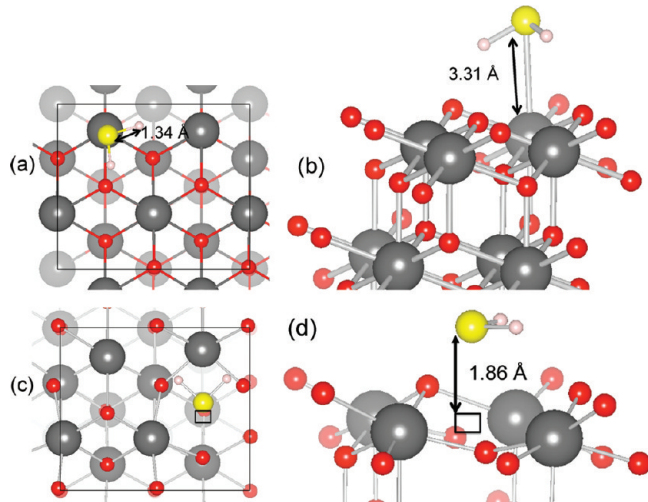


Figure 2. Most favorable adsorption geometry for H_2S on a stoichiometric $\text{CeO}_2(111)$ surface: top view (a) and side view (b). The color code is red, silver, yellow, and gray for the oxygen, cerium, sulfur, and hydrogen atoms, respectively. Selected bond distances are reported. Most favorable adsorption geometry for H_2S on a reduced $\text{CeO}_2(111)$ surface: top view (c) and side view (d). The vacancy is represented by the black square.

oxide materials.⁵⁸ For the case of adsorption and dissociation, we also consider water molecules and focus on the similarities and differences in the ways H_2S and H_2O interact with ceria. A summary of the energy barriers and endothermicities for all the studied processes is reported in Table 5 at the end of the Results section.

Adsorption. Stoichiometric $\text{CeO}_2(111)$ Surface. The most stable adsorption geometry for one H_2S molecule on the $\text{CeO}_2(111)$ surface is shown in Figure 2a and b. The sulfur atom sits on top of an undercoordinated Ce cation, with a bond distance of 3.31 Å, while the two hydrogen atoms form a hydrogen bond with the two neighboring oxygen ions. This configuration is in agreement with the DFT calculations by Chen et al.³⁸ and has an adsorption energy of $E_{ad} = -0.18$ eV.⁵⁹ Such a weak adsorption is in good agreement with the low desorption temperature (155 K) observed by Mullins et al. for H_2S on stoichiometric CeO_2 .²⁷ Other adsorption configurations (for example, a H_2S on top of an oxygen atom or on bridging positions) were found to have smaller adsorption energies. H_2O adsorbs on $\text{CeO}_2(111)$ in a similar fashion (see Supporting Information), with the only difference being a greater adsorption energy ($E_{ad} = -0.51$ eV). This value is in good agreement with experiments⁶⁰ and previous DFT+U studies.^{40,42,45} From these results, should a stoichiometric $\text{CeO}_2(111)$ surface be exposed to a mixture of H_2S and H_2O , as is the case in some oil-field environments, it mostly would favor water adsorption.

Reduced $\text{CeO}_2(111)$ Surface. The creation of a surface vacancy significantly affects the adsorption characteristics of CeO_2 . The most stable adsorption geometry for a surface with an oxygen vacancy is shown in Figure 2c and d. In this case, the sulfur ion adsorbs on top of the oxygen vacancy, as indicated by the black square. The distance between the vacancy (the vacancy position was taken as the position of the surface oxygen, which was removed to create the vacancy) and the sulfur (indicative of the distance between the surface and the adsorbate) is only 1.86 Å—smaller compared to the Ce–S bond distance of 3.31 Å.

Table 3. Adsorption Energies for an H₂S Molecule for Different Coverages^a

coverage (ML)	E_{ad} (eV)	$E_N - E_{N-1}$
0.25	-0.18	
0.50	-0.23	-0.28
0.75	-0.15	-0.01
1.0	-0.13	-0.07

^a The last column reports the difference, $E_N - E_{N-1}$, between the energy gain for a system of N adsorbed molecules (with respect to the case when these molecules are in the gas phase) relative to the energy gain for a system with $N - 1$ adsorbed molecules.

found on the stoichiometric ceria. This means that the sulfur atom is strongly attracted to the vacant site and minimizes its distance from it. The two hydrogen atoms orient themselves toward the nearest oxygen atoms. The adsorption energy for this configuration is $E_{\text{ad}} = -0.55$ eV, more than three times the adsorption energy for the stoichiometric surface, consistent with the shorter adsorbate–surface distance, as defined above.

A behavior similar to the one shown above for H₂S is found for H₂O (see Supporting Information). The oxygen ion is attracted to the vacant site and minimizes its distance from the surface. Due to the smaller size of oxygen compared to sulfur, the vacancy–oxygen distance is 1.07 Å. The adsorption energy for this configuration is $E_{\text{ad}} = -0.8$ eV, in good agreement with the results from Watkins et al.,⁴¹ but smaller than the one calculated by Fronzi et al.⁴² Some of the previous calculations,^{40–42} including those by Fronzi et al., were done without a +U correction. For comparison purposes, the adsorption energy that we calculated for this configuration, without the U term, is $E_{\text{ad}} = -0.66$ eV. This proves that, while the adsorption energies are affected by the Hubbard term significantly, this, however, cannot explain the high adsorption energy value obtained by Fronzi et al.⁴² When performing the structural relaxation to optimize this configuration, sometimes a dissociated H₂O molecule (two OH[−] radicals on the surface) is favored as the final state. This indicates that the dissociation of an H₂O molecule on a reduced CeO₂(111) surface is facile, and this will be further discussed in the next section.

Finally, it is worth noting that the adsorption energies for H₂S and H₂O are closer to each other on the reduced ceria than they are for a stoichiometric ceria surface. This means that the reduction state of the ceria surface changes the balance between the adsorbed H₂O and H₂S concentrations, and the difference between equilibrium adsorption tendencies between the two molecules is less marked on reduced ceria. (See Discussion for our interpretation of this result.)

Coverage Effects on the Stoichiometric CeO₂(111) Surface. We assessed the effects of coverage on the adsorption characteristics for a H₂S molecule for four different coverages, ranging from one to four H₂S molecules adsorbed on the stoichiometric CeO₂(111) slab, which correspond to 0.25–1.0 ML. These are reported in Table 3, which shows that adsorption energies are significantly affected by the coverage. While the adsorption energy increases for the two molecules on the surface compared to the case of a single molecule, the addition of a third and fourth molecule lowers the average adsorption energy. The last column in Table 3 reports the difference between the energy gain for a system of N adsorbed molecules (with respect to the case when these molecules are in the gas phase) relative to the energy gain

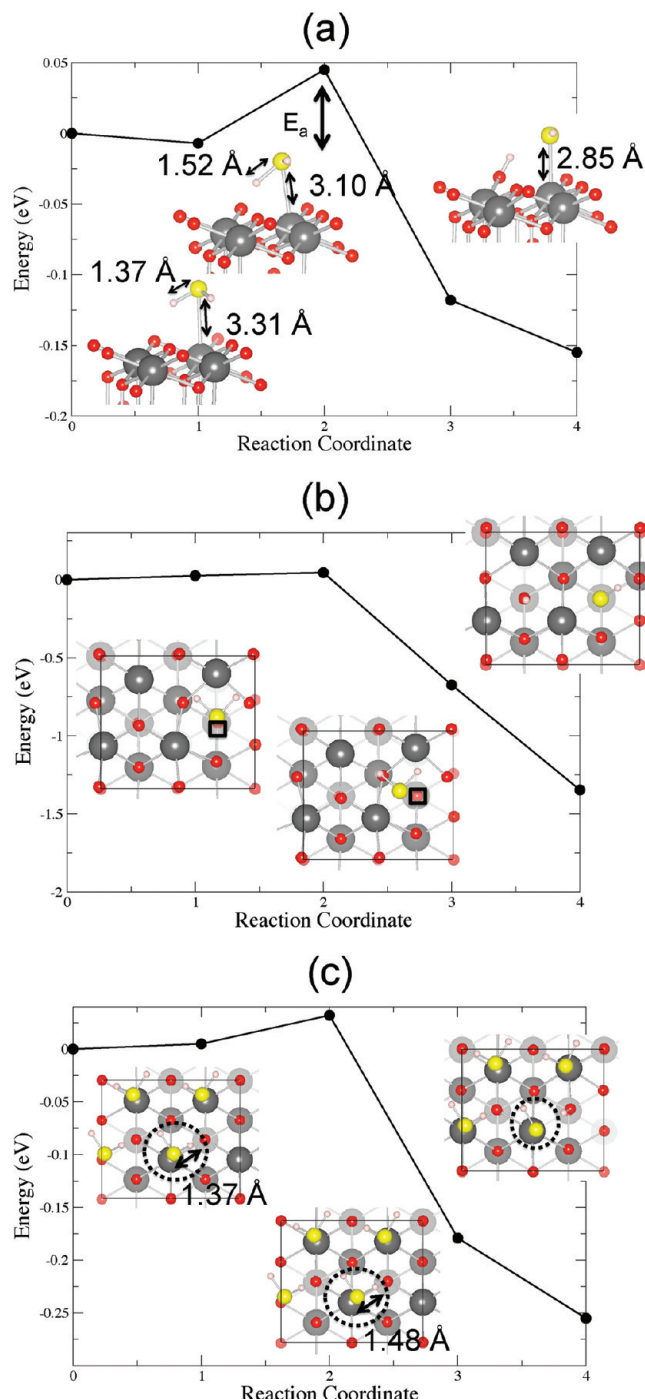


Figure 3. Minimum energy path for H₂S dissociation on stoichiometric CeO₂(111) (a), reduced CeO₂(111) (b), and stoichiometric CeO₂(111) with 1.0 ML coverage (c). The three snapshots correspond to the initial state (left), saddle point (center), and final state (right). The dotted circle in (c) highlights the H₂S molecule that dissociates. Some selected bond distances are reported. Color code as in Figure 2.

for a system with $N - 1$ adsorbed molecules. This quantity gives an indication of whether it is energetically favorable to adsorb another molecule on the surface (a negative value meaning it is favorable, while a positive one indicates the contrary). Our calculations predict that four H₂S molecules can be stably adsorbed on our slab. This is in good agreement with Mullins

Table 4. Charges Associated with H, OH, and SH in Figure 3a^a

radical	charge/e
OH ⁻	-0.74
SH ⁻	-0.30
H ⁺ (in OH ⁻)	0.68
H ⁺ (in SH ⁻)	0.67

^a These were calculated using the LORBIT=5 keyword in VASP and the following values for the Wigner–Seitz radii, 1.50, 1.50, 0.450, and 1.95 Å for oxygen, cerium, hydrogen, and sulfur, respectively.

et al.’s finding²⁷ that stoichiometric ceria at low temperatures (100 K) has a sulfur coverage of approximately 10 nm⁻², which is close to that of our simulation cell with four H₂S molecules ($4 \text{ S}/(0.78 \times 0.66 \text{ nm}) = 7.8 \text{ nm}^{-2}$).

In the case for H₂O adsorption, coverage does not affect the adsorption energies for the studied coverage range here. The adsorption energy obtained for a 1.0 ML coverage (corresponding to four molecules on the surface) is $E_{\text{ad}} = -0.55 \text{ eV}$, which is very close to the value obtained for a single adsorbed molecule. This is in agreement with previous calculations.^{40,42} A reason for this could be related to the smaller size of the H₂O molecule compared to the H₂S, which render the intermolecule interactions much weaker for the H₂O adsorption and therefore do not sterically hinder the adsorption with increasing coverage.

Dissociation. *Stoichiometric CeO₂(111) Surface.* The starting configuration for the dissociation reaction was the one described above for the adsorption—a H₂S molecule adsorbed on top of a Ce cation (see Figure 2a). The molecule was then dissociated into HS and H, by stretching one of the H–S bonds until the hydrogen binds to a neighboring oxygen and leaves behind a HS bound to the cerium cation in the final state. The dissociation process is shown in Figure 3a (see also the Supporting Information) where we report the Minimum Energy Path for the dissociation of H₂S, calculated by means of the climbing image NEB method. At the saddle point, the S–H bond distance is stretched by 10%, while the S–Ce one is contracted by 7%. The overall dissociation process is exothermic ($-0.15 \text{ eV}/\text{molecule}$) and virtually barrierless, with an energy barrier of $E_a = 0.05 \text{ eV}$. This means that H₂S features dissociative adsorption on a stoichiometric CeO₂(111) surface. These values are in good agreement with the previous calculations by Chen et al.³⁸ A charge analysis of the H, SH, and OH in the final configuration in Figure 3a (see Table 4) shows that the hydrogen released onto the oxygen atom has a positive charge, and the HS/OH has a negative charge. Therefore, from this point on, we refer to them as a proton, H⁺, and as adsorbed radicals, HS⁻ and OH⁻, respectively.

The results obtained for water dissociation, on the other hand, do not indicate a barrierless dissociation. The MEP for this process is reported in the Supporting Information. Although the reaction pathway is quite similar, with a hydrogen bound to a neighboring oxygen atom and leaving an OH⁻ radical behind, the energetics is different. The complete process is endothermic ($0.14 \text{ eV}/\text{molecule}$) and presents an energy barrier of approximately 0.2 eV, in contrast with the exothermic and barrierless H₂S dissociation. This contrast is likely due to water’s stronger H–O bonds which makes the dissociation of H₂O inherently unfavorable on a stoichiometric CeO₂(111) surface.

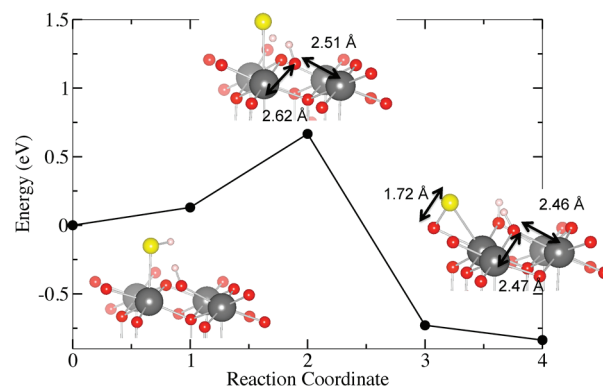


Figure 4. Minimum energy path for HS⁻ dissociation on CeO₂(111). The three snapshots correspond to the initial state (left), saddle point (center), and final state (right). Some selected bond distances are reported. Color code as in Figure 2.

The final step in this reaction is the second dehydrogenation via the dissociation of the remaining HS⁻ radical into S²⁻ and H⁺, shown in Figure 4. The initial configuration is the one with the HS⁻ radical bound to a Ce cation and the dissociated hydrogen forming a bond with the nearest oxygen. At the saddle point, the HS bond is stretched to 1.52 Å which suggests it is broken. The neighboring Ce and O ions show considerable structural relaxations, with some of the Ce–O bonds being stretched by 6%. In the final configuration, both hydrogen atoms are on top of an oxygen atom, forming two OH⁻ radicals with a bond distance of 0.97 Å. The sulfur atom moves toward one of the neighboring oxygens to form a bond with it, with a bond distance of 1.72 Å typical of a covalent bond. This configuration, which was first identified by Chen et al.,³⁸ is energetically favored by almost 1.20 eV over the configuration in which the sulfur atom remains on top of the Ce cation. Overall, this second dehydrogenation process is strongly exothermic, by -0.84 eV , and has an energy barrier of 0.69 eV. This means that, at sufficiently high temperatures, the H₂S molecule can dissociate on a CeO₂(111) surface by releasing both of its hydrogen atoms onto the surface.

In contrast, the second dehydrogenation process for H₂O (MEP available in the Supporting Information) is strongly endothermic, by 0.81 eV, and with an energy barrier $E_a = 0.81 \text{ eV}$. In the final state, the two protons bind to the two neighboring oxygen atoms, thus forming two OH⁻ radicals, while the O from the water molecule stays on top of the Ce cation. A configuration similar to the one found for HS⁻, where the sulfur forms a covalent bond with a neighboring oxygen (in this case with the remaining O approaching a neighboring surface oxygen), was found to be energetically unfavored.

In conclusion, the dissociation reaction characteristics of H₂S and H₂O on a stoichiometric CeO₂(111) are considerably different. While H₂S prefers to release both hydrogen atoms and the first one in a barrierless fashion, H₂O does not dissociate as easily on this surface. The potential reasons and the consequences of this finding to hydrogen embrittlement are discussed in the Discussion section of this paper.

Reduced CeO₂(111) Surface. As in the case of adsorption, the presence of vacancies on the ceria surface favorably affects the dissociation process. The minimum energy path for the first dehydrogenation of an adsorbed H₂S is shown in Figure 3b. The starting configuration has a H₂S molecule bound to the surface vacancy, as shown in Figure 2c. In the final configuration, the H₂S

molecule is dissociated into a HS^- and a OH^- radical. The saddle point corresponds to a configuration in which the whole H_2S is shifted toward the neighboring oxygen before releasing a hydrogen onto it. The energetics of this reaction is different from the one observed for a stoichiometric surface. The entire process is more strongly exothermic, with a final energy gain of -1.35 eV and again virtually no migration barrier ($<0.05 \text{ eV}$), meaning that H_2S dissociates right away, upon adsorbing onto a reduced $\text{CeO}_2(111)$ surface.

The MEP for the H_2O dissociation on the surface with a vacancy is reported in the Supporting Information. This process is also strongly exothermic, by -1.40 eV , and virtually barrierless. This explains our observation (see previous section on H_2O adsorption on a reduced $\text{CeO}_2(111)$ surface) that the water molecule dissociates even during some of the structural relaxations performed to find the most stable adsorption geometry. Our finding is also in agreement with the results obtained by Watkins et al.⁴¹ but at odds with those from Fronzi et al.,⁴² who find an energy barrier of 2.34 eV for this process. In the Supporting Information, we show how this contradiction with Fronzi et al.'s results might arise from some technical issues with their NEB calculations.

Coverage Effects on the Stoichiometric $\text{CeO}_2(111)$ Surface. Different coverage effects on the dissociation of H_2S were assessed by comparing the case for one adsorbed H_2S to the case with four adsorbed H_2S molecules on the stoichiometric $\text{CeO}_2(111)$ surface, corresponding to a coverage of 0.25 and 1.0 ML, respectively. This is reported in Figure 3c. Starting from a configuration in which the four molecules are adsorbed atop the Ce cations on the surface, one molecule was dehydrogenated by placing the hydrogen atom on top of a neighboring oxygen. The saddle point corresponds to a configuration in which the S–H bond is stretched by 8% and the entire H_2S molecule is shifted toward the oxygen atom. The energetics of this process is similar to the case when only one H_2S molecule was present on the surface. This process is also virtually barrierless, $E_a = 0.03 \text{ eV}$, and has an exothermicity of $-0.26 \text{ eV}/\text{molecule}$. It is worth noting that the exothermicity for this high coverage case is almost twice that for the one H_2S molecule case, suggesting that the presence of other H_2S molecules on the surface favors dissociation. A similar effect of coverage on dissociation energies has been observed for TiO_2 .⁶¹ This can be understood from the extent of steric repulsion between the sulfur atoms on the surface before and after dissociation of a H_2S . The average distance between the S^{2-} highlighted by the black circle in Figure 3c and the other S^{2-} atoms is 3.83 \AA before dissociation and 3.97 \AA after dissociation. It is clear that dissociating one H_2S molecule increases the average $\text{S}^{2-}–\text{S}^{2-}$ distance and therefore reduces their steric interactions, thus leading to a greater exothermicity for this reaction.

Hydrogen Absorption. Stoichiometric $\text{CeO}_2(111)$ Surface. The most important process leading to hydrogen embrittlement is the absorption/incorporation of the released hydrogen (which is present as a proton) into a subsurface position,¹¹ that is, an interstitial site in the case of stoichiometric ceria. The MEP for hydrogen absorption is shown in Figure 5a. The starting configuration is the one with a HS^- radical bound to a Ce cation and a OH^- radical on the surface. The hydrogen of the OH^- radical penetrates into the subsurface, by simply rotating by approximately 180° , as indicated by the arrow in Figure 5a. The saddle point for this process corresponds to a configuration in which the hydrogen has just crossed the oxygen plane on the surface. In the final configuration, the proton has completed this rotation and resides below the oxygen plane. This

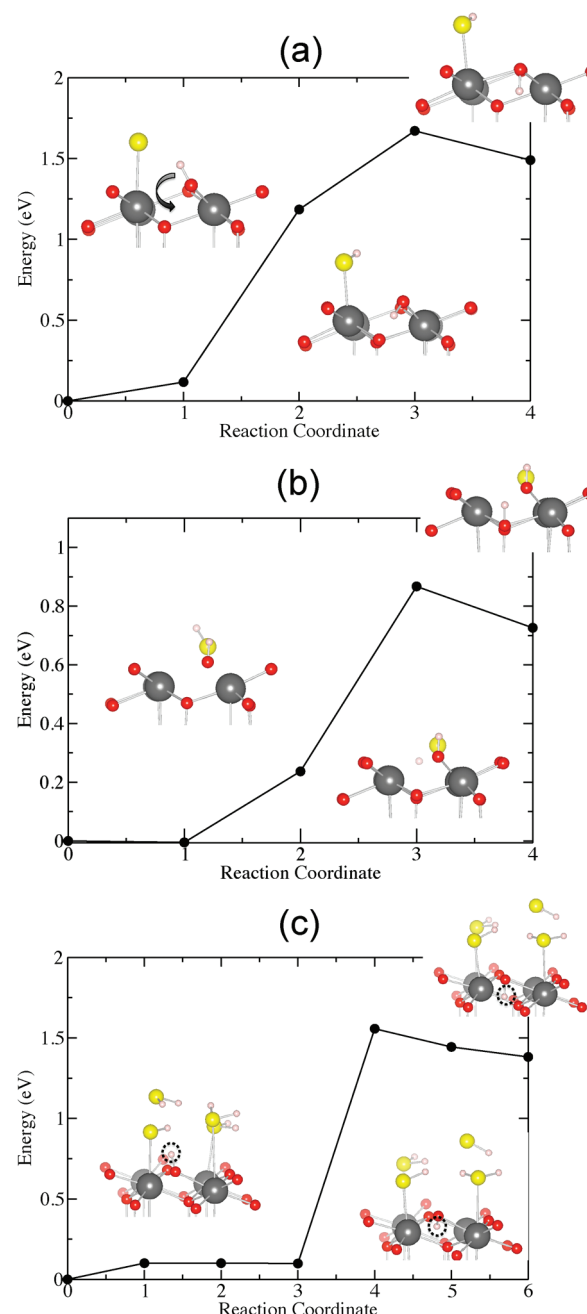


Figure 5. Minimum energy path for H^+ absorption in stoichiometric $\text{CeO}_2(111)$ (a), reduced $\text{CeO}_2(111)$ (b), and for 1.0 ML H_2S coverage (c). The three snapshots correspond to the initial state (left), saddle point (middle), and final state (right). Dashed circles are a guide to the eye for the hydrogen positions. Selected distances are reported. Selected bond distances are reported. Color code as in Figure 2.

process is highly endothermic (1.50 eV) and has an energy barrier of 1.67 eV , showing that hydrogen absorption into the subsurface is very unfavorable in stoichiometric ceria.

Subsequent to the subsurface absorption is the dissolution of a proton into the bulk of ceria. Here we define the dissolution energy as the energy difference between a configuration in which the proton is in the subsurface (the final point of Figure 5a) and another one in which the proton is in the bulk of the film.⁶² Here this energy is 0.67 eV —that is, even more energy beyond the

1.50 eV absorption endothermicity has to be supplied to move the proton into the bulk of the ceria. On the other hand, once in the bulk, the migration of proton is rather facile, with a calculated migration energy of 0.52 eV. This suggests that proton absorption into ceria is a surface-limited process, not a bulk diffusion limited process, and that ceria might be a good protective coating to prohibit hydrogen embrittlement of the coated metals thanks to its surface serving as a barrier to hydrogen absorption.

Reduced CeO₂(111) Surface. In Figure Sb we report the MEP for hydrogen absorption in the case of defective ceria. The starting configuration is the one with a HS⁻ radical bound onto the oxygen vacancy and a OH⁻ radical on the surface (see final state in Figure 3b). The hydrogen from the HS⁻ radical migrates toward a subsurface oxygen and eventually binds to it. The energetics of this process differs significantly from the stoichiometric case. Its endothermicity is only 0.72 eV, and the migration barrier is reduced to 0.86 eV, thus favoring hydrogen absorption significantly more than the case without the presence of surface vacancies. The consequences of this finding will be discussed in the next section.

Since there is experimental evidence for the presence of not only surface vacancies but also *subsurface* vacancies in ceria,^{24,25} we decided to study the effects of the latter on the hydrogen absorption process. In the Supporting Information, we show the MEP for this process. The starting configuration is the one with a HS⁻ radical bound onto a Ce cation and a OH⁻ radical on the surface. The hydrogen of the adsorbed OH⁻ radical then penetrates into the subsurface and binds to the oxygen vacancy. This process is strongly endothermic, by 1.66 eV, and has an energy barrier of 2.81 eV. It is clear that this pathway is energetically unfavored, compared to the previous one.

Coverage Effects on the Stoichiometric CeO₂(111) Surface. Similarly to the dissociation process, the effects of coverage on the hydrogen absorption process were assessed by comparing the case of one H₂S molecule (0.25 ML) to the case of four H₂S molecules (1.0 ML) adsorbed on the surface. This is reported in Figure 5c. In the starting configuration, one of the H₂S molecules is dissociated into SH⁻ and H⁺. This hydrogen then penetrates into the subsurface. The saddle point corresponds to the hydrogen having just crossed the oxygen plane. In the final configuration, the hydrogen has completed its rotation and is now below the oxygen plane. This pathway resembles very closely the one for a 0.25 ML cover, the only difference being that more molecules are present on the surface. The energetics of this process differs little from the case of a single H₂S molecule considered above. The energy barrier is $E_a = 1.55$ eV, a slightly smaller value than that of the single H₂S molecule case, suggesting a weak influence of the surface coverage on the ease of hydrogen absorption. The process is still strongly endothermic by 1.38 eV. In conclusion, coverage seems to affect hydrogen absorption only weakly, whereas surface vacancies have a considerable effect on the energetics of this process.

Reaction Mechanisms Leading to SO₂, H₂O, and H₂ Formation. Upon the dissociation of a H₂S molecule on the ceria surface, a series of reactions are possible, leading to the release of a H₂, H₂O, or SO₂ molecule (see Figure 1), as indicated by Chen et al. and Mullins et al.^{27,38} Understanding these reactions is of paramount importance because some of them lead to the creation of vacancies on the oxide surface. As we have already shown in this paper, vacancies strongly degrade the protective traits of ceria against H₂S dissociation and hydrogen absorption. In their study, Chen et al. found that the SO₂-forming pathway

is the most energetically favorable, with an exothermicity of -0.40 eV.³⁸ As it was commented in the Introduction, this fact is at odds with the results from Mullins et al., who found no evidence of SO_x formation.²⁷ To understand the reason for this contradiction, we re-evaluated the reaction pathways leading to the formation of these molecules for both a stoichiometric and reduced CeO₂(111) surface.

Stoichiometric CeO₂(111) Surface. The energy landscape for these processes on stoichiometric ceria and the snapshots of intermediate states are shown in Figure 6. The first three processes in Figure 6b are the ones which were described above, i.e., H₂S adsorption (M1), first dehydrogenation (M2), and second dehydrogenation (M3), and are common to all three reactions. Following these processes, three different reactions can take place, leading to the formation and evolution of H₂, H₂O, or SO₂ molecules. The black line in Figure 6a shows the water-forming pathway. Once both hydrogen atoms are released on the surface (M3), one hydrogen breaks its bond from the surface oxygen and binds to the neighboring OH⁻ radical, as shown by the black arrow in (M4), thus forming a H₂O molecule which is bound to the surface. This process, governed by the migration of the hydrogen from one OH⁻ to the other, presents a very high energy barrier (3.20 eV) and is only slightly exothermic (-0.28 eV). The final step is the release of the water molecule, which costs another 1.1 eV. The water-formation process leaves a vacancy on the CeO₂(111) surface and presents an endothermicity of 0.83 eV, compared to the starting configuration, and an energy barrier of 3.20 eV. If the sulfur atom left on the surface is placed on the vacancy, this configuration becomes slightly exothermic (-0.31 eV). However, this process is also kinetically unfavorable since its energy barrier is 3.2 eV. The SO₂ forming pathway is indicated by the red curve in Figure 6a. Starting from M3, the sulfur atom, which has already formed one covalent bond with a neighboring oxygen, forms another covalent bond with the other neighboring oxygen atom and pulls these two closer (shown by the blue arrow in M3). In the final configuration, M5, a SO₂ molecule is formed on the ceria surface. This formation process is moderately endothermic (less than 0.1 eV) and presents a relatively small energy barrier of 0.83 eV. The release of the SO₂ molecule, however, costs an additional 1.96 eV and is endothermic, compared to the starting configuration, by 0.92 eV. This process creates two vacancies on the ceria surface, a rather high vacancy concentration in this unit cell, and leads to strong rearrangements of the other atoms (see also the Discussion section). Finally, the last reaction is the one leading to H₂ formation. Starting from M3, both hydrogen atoms break their bonds from the oxygens and move toward each other to form a H₂ molecule, weakly bound to the surface Ce cation (see red arrows in M3). This process has a very large energy barrier of 4.10 eV and is endothermic by 1.00 eV. The final step is the release of the H₂ molecule which only costs 0.20 eV since the molecule is weakly bound to the surface.

In conclusion, we find that none of the studied reaction mechanisms is energetically favorable since they all present energy barriers greater than 1.90 eV and endothermicities of about 1.0 eV (with the exception of H₂O formation, which becomes slightly exothermic when the sulfur atom is placed in the vacancy). This finding differs significantly from what Chen et al. observed computationally and might seem in contradiction with the experimental findings from Mullins et al., where water formation is observed. In the next sections, we will show how these reaction pathways are influenced by the presence of surface

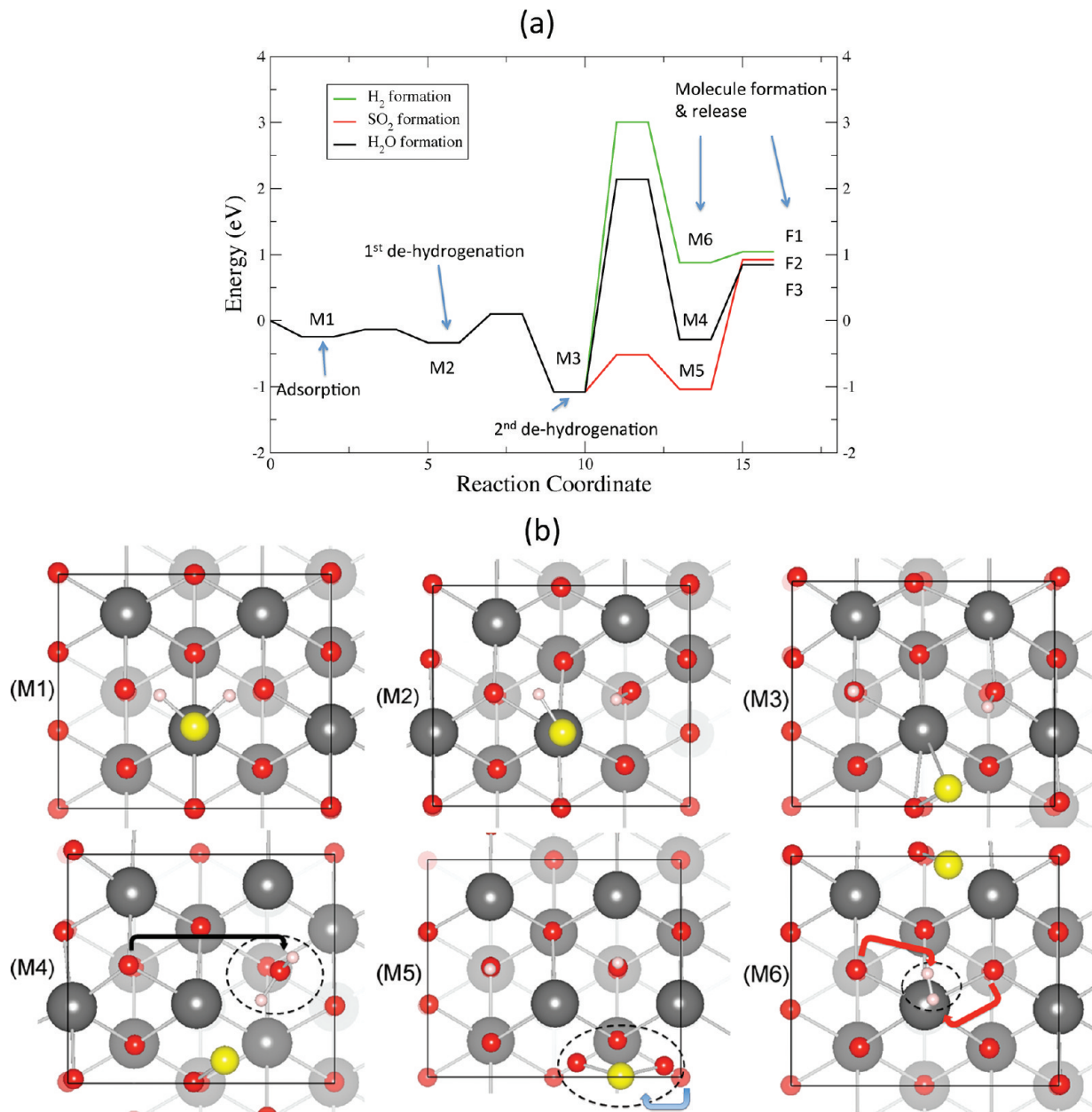


Figure 6. Energy landscape for the reaction pathways leading to H_2O , SO_2 and H_2 formation (a). Intermediate configurations (b) for the reaction pathways shown in (a). These correspond to the adsorption of H_2S (M1), first dehydrogenation (M2), second dehydrogenation (M3), water formation (M4), SO_2 formation (M5) and H_2 formation (M6). The dashed circles are a guide to the eye to locate the H_2O , SO_2 and H_2 molecules formed on the $CeO_2(111)$ surface. The black, blue and red arrows in (M4), (M5) and (M6) clarify the hydrogen/oxygen pathway for that specific reaction. Color code as in Figure 2.

vacancies, and in the Discussion section we will demonstrate that our calculations can actually explain the experimental evidence more accurately than the computational results reported by Chen et al.³⁸

Reduced $CeO_2(111)$ Surface. In this section, we focus on the effect that a surface vacancy has on the H_2O and H_2 creation and evolution pathways. SO_2 formation is not reported here because this process would remove three out of the four oxygens present on the surface, and thus, we expect it to be extremely energetically unfavorable. The energy landscape for the H_2O and H_2 formation reactions, now with a surface vacancy, and the snapshots of the intermediate states are reported in Figure 7. The

energetics differ significantly from the stoichiometric case. The first two processes are the H_2S adsorption (M1) and first dehydrogenation (M2), which were described above and are common to both pathways. The black lines shows the water-formation pathway. Starting from M2, the hydrogen of HS^- breaks its bond from sulfur and moves to the neighboring OH^- radical, thus forming an adsorbed water molecule on the surface. This process costs 0.82 eV and is barrierless. The final step of the water formation process is the release of this molecule into the vacuum (F1), costing another 0.97 eV. Here the water formation pathway is slightly exothermic (-0.15 eV/molecule), compared with the initial configuration, in contrast with stoichiometric

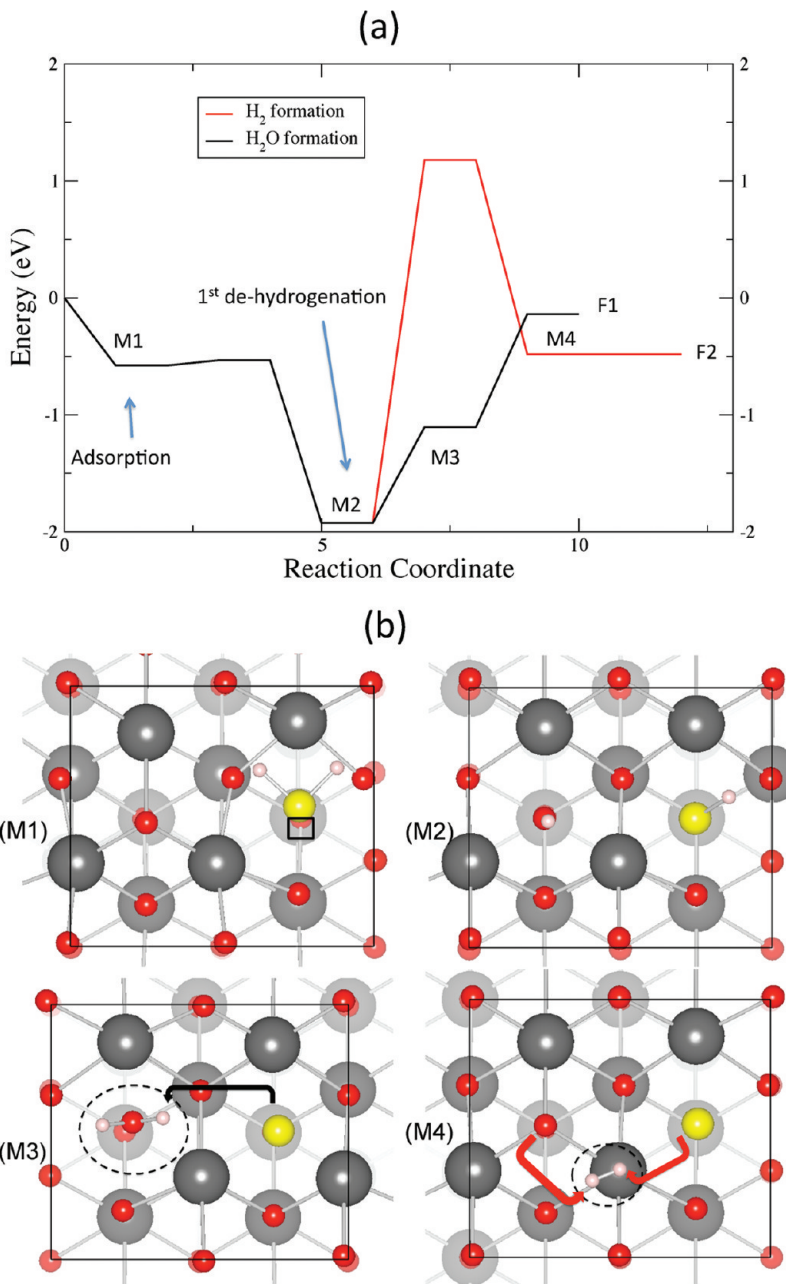


Figure 7. Energy landscape for the reaction pathways leading to H_2O , SO_2 and H_2 formation (a) on a reduced ceria surface. These correspond to, (b), the adsorption of H_2S on a surface vacancy (M1), first dehydrogenation (M2), second dehydrogenation (M3), water formation (M4) and H_2 formation (M5). The dashed circles indicate the H_2O and H_2 molecules formed on the reduced $\text{CeO}_2(111)$ surface. Color code as in Figure 2.

ceria, on which it was endothermic by 0.83 eV. The highest energy barrier associated with this process is 1.79 eV (since the $\text{M}2 \rightarrow \text{M}3$ process is barrierless, we estimate the highest energy barrier as the energy difference between $\text{M}2$ and $\text{F}1$). We believe that the reason for the smaller barrier and exothermicity is the breaking of a relatively weaker $\text{H}-\text{S}$ bond compared to the $\text{O}-\text{H}$ bond on stoichiometric ceria prior to water formation (see also Discussion).

The H_2 formation process starts from $\text{M}2$ in Figure 7a, with a OH^- and a SH^- radical on the surface. Both hydrogen atoms break their bond with the S and O (as indicated by the red arrows) and move toward the center to create a H_2 molecule ($\text{M}4$), which is weakly bound onto the Ce cation. The energy

barrier associated with this process is rather high, $E_a = 3.12$ eV, and following this, the H_2 molecule desorbs, without any energy cost, from the surface ($\text{F}2$). The overall H_2 formation pathway is exothermic by 0.5 eV, compared to the initial state, and presents an energy barrier, $E_a = 3.12$ eV.

Our calculations reported here demonstrate that the presence of a surface vacancy strongly affects the energetics of these reaction pathways, making both of them more favored. In light of our results, water formation on the reduced $\text{CeO}_2(111)$ surface is possible. H_2 formation was also found to be exothermic, but the energy barrier is too high to observe this reaction with discernible kinetics at room temperature. These findings are discussed further in the next section. In Table 5 we

Table 5. Summary of the Energy Differences and Energy Barriers between the Initial and Final Configurations for Each Studied Reaction^a

reaction	ΔE (eV)	E_a (eV)
H ₂ S adsorption	-0.18	0.00
H ₂ O adsorption	-0.52	0.00
H ₂ S adsorption (vacancy)	-0.55	0.00
H ₂ O adsorption (vacancy)	-0.80	0.00
H ₂ S adsorption (full coverage)	-0.13	0.00
H ₂ S first dehydrogenation	-0.16	0.19
H ₂ O first dehydrogenation	0.14	0.20
H ₂ S second dehydrogenation	-1.20	0.69
H ₂ O second dehydrogenation	0.81	0.81
H ₂ S first dehydrogenation (vacancy)	-1.35	0.05
H ₂ O first dehydrogenation (vacancy)	-1.40	0.05
H ₂ S first dehydrogenation (full coverage)	-0.26	0.03
hydrogen absorption	1.50	1.67
hydrogen absorption (vacancy)	0.72	0.86
hydrogen absorption (full coverage)	1.38	1.55
hydrogen dissolution	0.67	-
hydrogen diffusion	0.00	0.52
H ₂ O formation	0.83	3.20
H ₂ formation	1.20	4.10
SO ₂ formation	0.92	1.90
H ₂ O formation (vacancy)	-0.15	1.79
H ₂ formation (vacancy)	0.92	3.12

^a A negative energy difference is for exothermic, and a positive one is for endothermic reactions. Energy barriers for reactions with barrierless steps are taken as the energy difference between the lowest and highest energy step (for instance, in the case of H₂O formation on reduced ceria, the energy barrier is the energy difference between M2 and F1; see above and Figure 7a).

report a summary of the energetics for all the reactions studied in this work.

■ DISCUSSION

Protection against Hydrogen Embrittlement. One main aim of this paper was to assess the protective properties of ceria against hydrogen penetration, upon being subjected to H₂S and H₂O. For this material to be protective against hydrogen embrittlement, at least one of the processes leading to hydrogen penetration into the underlying metal (adsorption, dissociation, and hydrogen absorption and diffusion) must be significantly hindered. From our results it is clear that stoichiometric ceria presents the best protective properties. Indeed, stoichiometric ceria presents a high energy barrier (1.67 eV for 0.25 ML coverage) for proton absorption on its subsurface, which renders the entire *hydrogen penetration process surface-absorption limited*. Such a high energy barrier would not permit significant hydrogen absorption to take place at 50–200 °C, which is the temperature of interest for oil production and exploration field applications. Furthermore, in a mixed H₂S/H₂O environment (as is the case in the deep drilling fluids of an oil field), the adsorption on CeO₂(111) is dominated by H₂O, and this is the species that is more difficult to dissociate and release hydrogen compared to the H₂S. In a recent paper, Johnson and Carter¹¹ characterized the ability of two surface alloys, FeAl and Fe₃Si, to prevent

hydrogen absorption into steel. They found Fe₃Si to be the most effective at inhibiting hydrogen absorption, with a barrier of 1.91 eV for proton absorption on the (1 1 0) surface and a 0.79 eV endothermicity to bulk dissolution, compared to the pure Fe(110) surface with a 1.02 eV barrier and 0.20 eV dissolution energy. A comparison to CeO₂(111), with an energy barrier of 1.67 eV (here we use the value we obtained for stoichiometric ceria with one molecule on the surface (0.25 ML) since this is the same as the coverage used in their work¹¹) for proton absorption on its surface and endothermicity to bulk dissolution of 2.17 eV⁶³ shows that such an oxide layer could provide a better protection against hydrogen embrittlement of the underlying alloy, mainly because of the higher endothermicity of the dissolution process. The drawback of such oxide coatings compared to the integrated surface alloys, as Fe₃Si, would be their adhesion and durability issues.

In this work, vacancies were found to strongly degrade the protective properties of this material. Indeed, the increase in the adsorption energies of both molecules, observed in the presence of vacancies, favors the adsorption of more of H₂S and H₂O on the surface. Once on the surface, these dissociate more easily (since vacancies strongly favor dissociation) and therefore release more protons onto the surface. The released protons are then able to diffuse into the subsurface since the absorption barrier for this process is significantly lower. From these considerations, it is clear that reducing ceria has a negative effect on its protective properties against hydrogen penetration and that vacancies must be avoided. This can be achieved by tailoring the synthesis conditions with high oxygen pressures to minimize the presence of vacancies, although the conditions in which it could serve as a coating (as such in oil drilling and exploration) are not as controllable. It is worth noting, however, that, regardless of the presence of vacancies, hydrogen penetration in CeO₂(111) is always a surface-limited process.

One of the main findings of this work is that H₂S and H₂O behave differently on a stoichiometric CeO₂(111) surface. Water, for instance, adsorbs more strongly than H₂S (its adsorption energy is three times larger). On the other hand, water does not spontaneously dissociate on ceria, while H₂S does. Interestingly, a similar difference between H₂S and H₂O has been observed on rutile TiO₂(110), where the adsorption of H₂O is stronger than that of H₂S by 0.32–0.58 eV^{61,64} and the dissociation is more endothermic by 0.05–0.29 eV.^{61–65} This has important consequences for HE. We believe this trend with the easier dissociation of H₂S compared to H₂O is related to the different strengths of the H–O and H–S bonds of the molecular species. To rationalize this, we computed and compared the energy required to dissociate these molecules when they are in the gas phase. Energies of 4.16 and 5.61 eV are required to split a H₂S and a H₂O molecule into HS[−] + H⁺ and HO[−] + H⁺, respectively. This shows that the H–S bond in H₂S is weaker than the O–H in water, and this, in turn, explains the different dissociative properties of these molecules. From this, we conclude that the easier dissociation of the H₂S is governed, mainly, by the intrinsic difference between the H–S and H–O bond strengths and not by specific features of the oxide surface, as testified by the fact that the same behavior is observed on rutile TiO₂(110) as well as on CeO₂(111). This finding provides a qualitative explanation for why hydrogen embrittlement in steel and related alloys is more severe when H₂S is present in the fluid environment.^{13,14} Steels and alloys form a native protective oxide layer (unless the environment is strongly reducing). Assuming

that these native oxide surfaces behave in a qualitatively similar way to ceria and titania, we expect that H₂S dissociation will be more favorable than that of H₂O, thus making H₂S the main culprit for hydrogen release onto the surfaces.

Effects of Vacancies and Coverage. Our calculations have shown that vacancies have a strong influence on several of the interactions between H₂O/H₂S and CeO₂(111), described in Figure 1. Coverage, on the other hand, has only a weak effect on these processes. An interesting finding is that the difference in the behavior observed for H₂O/H₂S decreases significantly in the presence of a surface vacancy. When a vacancy is present on the CeO₂(111) surface, the adsorption energies for H₂O and H₂S differ by only 45% (as opposed to a 300% difference in the stoichiometric case), and dissociation is strongly exothermic (by approximately -1.40 eV) for both molecules. Here we provide a possible explanation for the effects that vacancies have on these processes, primarily on the basis of the predominance of Coulombic interactions. Using a simple ionic model, the interactions between these ions can be seen as a combination of a Coulombic ($(q_1 q_2)/(r)$) and a steric (Ae^{-ar}) interaction.⁴⁸ Because of their different ionic radii, 1.4 and 1.84 Å for oxygen and sulfur, respectively,⁶⁶ the intensity and range of the steric repulsion (as described by the A and a parameters) is different for these two species, while the radial dependence of the Coulombic interaction is the same since both species carry a formal charge of -2. Therefore, on stoichiometric CeO₂(111), the difference between the adsorption energies of these two molecules is a consequence of the different steric repulsion of these two species. The larger radius of S²⁻ results in a longer bond distance with Ce⁴⁺, compared to O²⁻, and thus a lower adsorption energy. When a vacancy is present on the surface, this causes a local accumulation of positive charge in its vicinity, which, in turn, results in an increased Coulombic attraction between this positive charge and the S²⁻(O²⁻) species of H₂S (H₂O). This increased electrostatic attraction well explains the higher values obtained for the adsorption energy in the presence of a vacancy, a phenomenon which is generally observed in several oxide materials.⁶⁷ The fact that the adsorption energies for H₂O and H₂S are much closer to each other in the presence of a vacancy can also be explained in terms of an ionic model. Indeed, because of the presence of a vacancy, the Coulombic interaction, which is the same for both molecules, becomes predominant over the steric repulsion, thus minimizing the differences between these two molecules.

Our results show that H₂S surface coverage affects rather weakly the interaction between H₂S and CeO₂(111). Perhaps the most significant effect is that H₂S dissociation becomes more exothermic for a 1.0 ML coverage than for the 0.25 ML, a consequence of the strong steric interaction between the molecules on the surface. A similar tendency was observed, by Harris et al., for the case of water dissociation on a rutile TiO₂(110) surface. Also, increased coverage slightly lowers the energy barrier and endothermicity (see Table 5) for hydrogen absorption into the subsurface. The effects of coverage have been usually neglected in similar studies,^{11,68} probably because when smaller molecules are studied, such as H₂O and H₂, their steric interaction is weaker and coverage effects are negligible because of their smaller size.^{40,42} In view of our results, we conclude, however, that coverage effects might have to be taken into account when considering large molecules, such as H₂S, or very high coverage values, >1.0 ML.

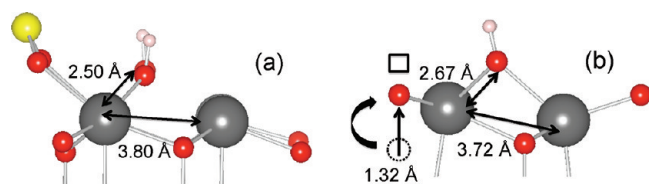


Figure 8. Side view of the CeO₂(111) slab before (a) and after (b) SO₂ release. These configurations correspond to M5 and F2 in Figure 6a. The dotted circle in (b) indicates the position of the oxygen atoms before the SO₂ removal. The black square indicates the surface oxygen vacancies formed after SO₂ release. Selected bond distances are reported. Color code as in Figure 2.

Reaction Pathways and Comparison with the Experimental Data. As explained in Figure 1, when an H₂S molecule is dissociated on the ceria surface, three different reactions might occur which lead to the production of H₂O, SO₂, and H₂. While H₂ formation and release from the surface to the environment is desirable, the formation of H₂O and SO₂ is not desirable as they reduce the surface. Chen et al. predicted that the SO₂-forming pathway is energetically most favorable.³⁸ In contrast, the experimental data by Mullins et al. show that, on stoichiometric ceria, some water is produced on the surface and released between 200 and 450 K. In Mullins' experiments, when ceria is reduced, more water is produced, and a clear desorption peak appears at 580 K. Finally, when ceria near the surface region is largely reduced up to ca. 70%, i.e., CeO_{1.65}, water formation is suppressed, and H₂ desorbs near 580 K. No evidence of SO_x release was observed throughout the temperature (100–800 K) and composition (2 ≤ x ≤ 1.55) intervals studied for CeO_x.²⁷ Our results on these three pathways for stoichiometric ceria show that none of them is energetically favorable. These reactions have very high energy barriers (>1.9 eV) and are strongly endothermic (>0.8 eV). This suggests that a fully stoichiometric CeO₂(111) surface exposed to H₂S does not produce either H₂O, SO₂, or H₂. We have to note that our results differ strongly from those of Chen et al.,³⁸ especially for the SO₂ forming reaction. We find the SO₂ release to be strongly endothermic, in contrast with their results. In Figure 8 we show a side view of the ceria surface before, (a), and after, (b), the SO₂ molecule has been released. Since the SO₂ release forms two vacancies on the surface, the neighboring ions undergo significant relaxations. Figure 8b shows that the subsurface oxygen atoms below the surface vacancies shift upward by 1.32 Å, thus getting closer to these vacancies. This shift, in turn, strongly affects the Ce–Ce and Ce–O bond distances, with significant bond length contractions/extensions of up to 7%. Such strong relaxations upon SO₂ formation explain well the high energy cost that this process has.

Our results are largely consistent with the experimental data from Mullins et al.²⁷ Indeed, they observe that, on stoichiometric ceria, no H₂ and SO₂ are formed, in agreement with our calculations. The little amount of water desorption observed by these authors is probably caused by the presence of a few surface vacancies and/or by the presence of water contaminants in the experimental analysis setup, as discussed by the authors themselves.²⁷ On the other hand, for reduced CeO₂(111), Mullins et al. observe a stronger water desorption with a well-defined peak at 580 K. Our results show that the highest energy barrier associated with this process is 1.79 eV. Using transition state theory formalism,⁶⁹ we can estimate the rate of this reaction of the form of an attempt frequency multiplied by a Boltzmann

factor, i.e.

$$\nu = \nu_0 \exp(E_a/k_B T)$$

where k_B is the Boltzmann constant and ν_0 is an attempt frequency. We take $\nu_0 = 10^{13}$ Hz, an appropriate value for most oxides.^{70–72} From this formula we find the range of temperatures at which the water formation should occur within a minimum range of frequencies 0.1–10 Hz, i.e., that this process happens on the second time scale corresponding to the experimental time scale. The temperature range we obtain is 640–750 K, not far from the experimentally measured 580 K for water desorption peak.

We believe that the transition from H₂O formation to H₂ formation in Mullins' experiments when ceria is largely reduced (by more than 70%) is related to the difficulty of removal of oxygen from the increasingly reduced surface. To confirm this, we compared the formation energies of a single vacancy and a second vacancy after the first one on the CeO₂(111) surface. These energies are 2.78 and 3.56 eV, respectively—the creation of a second vacancy costs an extra 0.78 eV, thus suggesting that, on largely reduced ceria, water production (which creates extra vacancies on the surface) is less favorable. The energy barrier for H₂ formation predicted by our calculations for this process is greater than 3.0 eV. This value is too high to justify the experimental data. However, as mentioned in the Introduction, when ceria is significantly reduced, it is not expected to be in the fluorite crystal structure,⁷ and there are indications that its surface is consistent with the bixbyite structure.⁴⁹ This structure presents strong relaxations of the oxygen ions and an ordering of the vacancies, both of which are expected to play a significant role on the energetics of H₂ formation. Also, our calculations consider a system with only one single vacancy, corresponding to a surface vacancy concentration of 25% and an overall stoichiometry of CeO_{1.95}. On the other hand, it is known experimentally that vacancies tend to form ordered clusters on the surface.²⁴ We expect that, if a larger system with more realistic vacancy concentrations and structures were considered, the energy barrier for this process could be lower. Such large computational cells are beyond the range of feasibility of DFT calculations and could be studied instead by using suitable interionic potentials,^{48,73} warranting future work on this topic.

CONCLUSIONS

In this paper, we studied the reaction mechanisms between the CeO₂(111) surface and the H₂S and H₂O molecules and the thermodynamic and kinetic energetics of these reactions, by using DFT+U calculations. The results were validated through a comprehensive comparison with the experimental data of Mullins et al.²⁷ We predict that the penetration of hydrogen into ceria upon H₂S/H₂O dissociation is limited by hydrogen absorption into the subsurface, with a very high energy barrier, $E_a = 1.67$ eV, and endothermicity, $\Delta E = 1.50$ eV. The subsequent hydrogen diffusion in ceria is rather facile, with a migration barrier of 0.52 eV. This result suggests that stoichiometric ceria can provide a high protection against hydrogen embrittlement of the underlying alloy, by blocking hydrogen absorption on its surface. We identified that, compared to H₂O, H₂S is the main culprit for hydrogen release onto the surface, and the reason for this behavior was explained on the basis of the intrinsic strength of the H–S and the H–O bonds of these molecules.

The presence of surface vacancies and, to a smaller extent, increasing H₂S coverage was found to favor most of the considered elementary reactions and, thus, to lessen the protective-ness of this material against hydrogen embrittlement. The reasons for the effects of vacancy and coverage on these reactions were discussed and interpreted in terms of the competition between the colomeric and steric interactions and local structural relaxations. Overall, we suggest that vacancies are avoided in ceria for the purpose of coating against hydrogen penetration, for example by tailoring the synthesis conditions with high oxygen pressures.

ASSOCIATED CONTENT

Supporting Information. Additional figures and text. This information is available free of charge via the Internet at <http://pubs.acs.org>

AUTHOR INFORMATION

Corresponding Author

*E-mail: byildiz@mit.edu

Present Addresses

[†]School of Chemistry, Trinity College Dublin, College Green, Dublin 2, Ireland.

ACKNOWLEDGMENT

DM would like to thank Mostafa Youssef (MIT) for fruitful conversations on NEB calculations. DM and BY acknowledge the National Science Foundation for computational support through the TeraGrid Advanced Support Program, with a Start-up allocation (TG-DMR100098) and a Research allocation (TG-DMR110004). This work was financially supported by the Schlumberger-Doll Research Center. All the figures in this paper were realized with the VESTA visualization software.⁷⁴

REFERENCES

- (1) Trovarelli, A. *Catalysis by Ceria and Related Materials*; Imperial College Press: London, 2002.
- (2) Steele, B.; Heinzel, A. *Nature* **2001**, *414*, 345–352.
- (3) Jacobson, A. J. *Chem. Mater.* **2010**, *22*, 660–674.
- (4) Abanades, S.; Flamant, G. *Sol. Energy* **2006**, *80*, 1611–1623.
- (5) Mullins, D.; Overbury, S. *Surf. Sci.* **2002**, *511*, L293–L297.
- (6) Etzell, T.; Flengas, S. *Chem. Rev.* **1970**, *70*, 339–&.
- (7) Mogensen, M.; Sammes, N.; Tompsett, G. *Solid State Ionics* **2000**, *129*, 63–94.
- (8) Flytzani-Stephanopoulos, M.; Sakbodin, M.; Wang, Z. *Science* **2006**, *312*, 1508–1510.
- (9) Jiang, D.; Carter, E. *J. Phys. Chem. B* **2004**, *108*, 19140–19145.
- (10) Jiang, D.; Carter, E. *Surf. Sci.* **2005**, *583*, 60–68.
- (11) Johnson, D. F.; Carter, E. A. *Acta Mater.* **2010**, *58*, 638–648.
- (12) Dadfarnia, M.; Novak, P.; Ahn, D. C.; Liu, J. B.; Sofronis, P.; Johnson, D. D.; Robertson, I. M. *Adv. Mater.* **2010**, *22*, 1128–1135.
- (13) Chernov, V. Y.; Makarenko, V. D.; Shlapak, L. S. *Mater. Sci.* **2003**, *39*, 144–147, DOI: 10.1023/A:1026151118353.
- (14) Eadie, R. L.; Szklarz, K. E.; Sutherland, R. L. *Corrosion* **2005**, *61*, 167.
- (15) Sarian, S.; Gibson, A. *Soc. Pet. Eng.* **2005**, 1–8.
- (16) Noonan, S.; Dowling, M.; Claczek, W.; Piers, K. *Soc. Pet. Eng.* **2009**, 1–8.
- (17) Seal, S.; Bose, S.; Roy, S. *Oxid. Met.* **1994**, *41*, 139–178.

- (18) Thanneeru, R.; Patil, S.; Deshpande, S.; Seal, S. *Acta Mater.* **2007**, *55*, 3457–3466.
- (19) Shirpour, M.; Gregori, G.; Merkle, R.; Maier, J. *Phys. Chem. Chem. Phys.* **2011**, *13*, 937–940.
- (20) Pfau, A.; Schierbaum, K. *Surf. Sci.* **1994**, *321*, 71–80.
- (21) Mullins, D.; Overbury, S.; Huntley, D. *Surf. Sci.* **1998**, *409*, 307–319.
- (22) Mullins, D.; Radulovic, P.; Overbury, S. *Surf. Sci.* **1999**, *429*, 186–198.
- (23) Zeng, Y.; Kaytakoglu, S.; Harrison, D. *Chem. Eng. Sci.* **2000**, *55*, 4893–4900.
- (24) Esch, F.; Fabris, S.; Zhou, L.; Montini, T.; Africh, C.; Fornasiero, P.; Comelli, G.; Rosei, R. *Science* **2005**, *309*, 752–755.
- (25) Gritschneider, S.; Reichling, M. *Nanotechnology* **2007**, *18*, 044024, International Conference on Nanoscience and Technology, Basel, Switzerland, JUL 30-AUG 04, 2006.
- (26) Torbruegge, S.; Reichling, M.; Ishiyama, A.; Morita, S.; Custance, O. *Phys. Rev. Lett.* **2007**, *99*, 653–658.
- (27) Mullins, D. R.; McDonald, T. S. *Surf. Sci.* **2007**, *601*, 4931–4938.
- (28) Hull, S.; Norberg, S. T.; Ahmed, I.; Eriksson, S. G.; Marrocchelli, D.; Madden, P. A. *J. Solid State Chem.* **2009**, *182*, 2815–2821.
- (29) Avila-Paredes, H. J.; Chen, C.-T.; Wang, S.; De Souza, R. A.; Martin, M.; Munir, Z.; Kim, S. *J. Mater. Chem.* **2010**, *20*, 10110–10112.
- (30) Avila-Paredes, H. J.; Zhao, J.; Wang, S.; Pietrowski, M.; De Souza, R. A.; Reinholdt, A.; Munir, Z. A.; Martin, M.; Kim, S. *J. Mater. Chem.* **2010**, *20*, 990–994.
- (31) Skorodumova, N. V.; Baudin, M.; Hermansson, K. *Phys. Rev. B* **2004**, *69*, 075401–8.
- (32) Fabris, S.; de Gironcoli, S.; Baroni, S.; Vicario, G.; Balducci, G. *Phys. Rev. B* **2005**, *71*, 653–658.
- (33) Fabris, S.; Vicario, G.; Balducci, G.; de Gironcoli, S.; Baroni, S. *J. Phys. Chem. B* **2005**, *109*, 22860–22867.
- (34) Nolan, M.; Grigoleit, S.; Sayle, D.; Parker, S.; Watson, G. *Surf. Sci.* **2005**, *576*, 217–229.
- (35) Nolan, M.; Parker, S.; Watson, G. *Surf. Sci.* **2005**, *595*, 223–232.
- (36) Vicario, G.; Balducci, G.; Fabris, S.; de Gironcoli, S.; Baroni, S. *J. Phys. Chem. B* **2006**, *110*, 19380–19385.
- (37) Nolan, M.; Parker, S.; Watson, G. *Phys. Chem. Chem. Phys.* **2006**, *8*, 216–218.
- (38) Chen, H.-T.; Choi, Y.; Liu, M.; Lin, M. C. *J. Phys. Chem. C* **2007**, *111*, 11117–11122.
- (39) Chen, H.-T.; Choi, Y. M.; Liu, M.; Lin, M. C. *Chem. Phys. Chem.* **2007**, *8*, 849–855.
- (40) Kumar, S.; Schelling, P. K. *J. Chem. Phys.* **2006**, *125*, 204704–12.
- (41) Watkins, M. B.; Foster, A. S.; Shluger, A. L. *J. Phys. Chem. C* **2007**, *111*, 15337–15341.
- (42) Fronzi, M.; Piccinin, S.; Delley, B.; Traversa, E.; Stampfl, C. *Phys. Chem. Chem. Phys.* **2009**, *11*, 9188–9199.
- (43) Ganduglia-Pirovano, M. V.; Da Silva, J. L. F.; Sauer, J. *Phys. Rev. Lett.* **2009**, *102*, 653–658.
- (44) Migani, A.; Neyman, K. M.; Illas, F.; Bromley, S. T. *J. Chem. Phys.* **2009**, *131*, 064701–8.
- (45) Yang, Z.; Wang, Q.; Wei, S.; Ma, D.; Sun, Q. *J. Phys. Chem. C* **2010**, *114*, 14891–14899.
- (46) Migani, A.; Vayssilov, G. N.; Bromley, S. T.; Illas, F.; Neyman, K. M. *Chem. Commun.* **2010**, *46*, 5936–5938.
- (47) Migani, A.; Vayssilov, G. N.; Bromley, S. T.; Illas, F.; Neyman, K. M. *J. Mater. Chem.* **2010**, *20*, 10535–10546.
- (48) Burbano, M.; Marrocchelli, D.; Yildiz, B.; Tuller, H. J.; Norberg, S.; Hull, S.; Madden, P.; Watson, G. *J. Phys.: Condens. Matter* **2011**, *23*, 255402–9.
- (49) Mullins, D.; Radulovic, P.; Overbury, S. *Surf. Sci.* **1999**, *429*, 186–198.
- (50) Kresse, G.; Hafner, J. *Phys. Rev. B* **1994**, *49*, 14251–14269.
- (51) Kresse, G.; Furthmuller, J. *Phys. Rev. B* **1996**, *54*, 11169–11186.
- (52) Olivier, P.; Parker, S.; Mackrodt, W. *Model. Simul. Mater. Sci.* **1993**, *1*, 755–760.
- (53) Henkelman, G.; Uberuaga, B.; Jonsson, H. *J. Chem. Phys.* **2000**, *113*, 9901–9904.
- (54) Norenberg, H.; Briggs, G. *Surf. Sci.* **1999**, *433*, 127–130, 14th International Vacuum Congress/10th International Conference on Solid Surfaces/5th International Conference on Nanometre-Scale Science and Technology/10th International Conference on Quantitative Surface Analysis, Birmingham, England, Aug 31–Sep 04, 1998.
- (55) Clausen, K.; Haynes, W.; MacDonald, J.; Osborn, R.; Schnabel, P.; Hutchings, M.; Magerl, A. *J. Chem. Soc., Faraday Trans. 2* **1987**, *83*, 1109–1112.
- (56) Nakajima, A.; Yoshihara, A.; Ishigame, M. *Phys. Rev. B* **1994**, *50*, 13297–13307.
- (57) Zhang, T.; Ma, J.; Huang, H.; Hing, P.; Xia, Z.; Chan, S.; Kilner, J. *Solid State Sci.* **2003**, *5*, 1505–1511.
- (58) Rashkeev, S. N.; Sohlberg, K. W.; Zhuo, S.; Pantelides, S. T. *J. Phys. Chem. C* **2007**, *111*, 7175–7178.
- (59) Density Functional Theory provides a poor representation of dispersion interactions. For this reason, adsorption energies are in general underestimated. In the current study, however, this does not represent a limitation since we are not interested in the absolute values of the adsorption energies but rather in the relative changes with the different geometries, molecules, coverages, and stoichiometries that are sampled.
- (60) Henderson, M.; Perkins, C.; Engelhard, M.; Thevuthasan, S.; Peden, C. *Surf. Sci.* **2003**, *526*, 1–18.
- (61) Harris, L.; Quong, A. *Phys. Rev. Lett.* **2004**, *93*, 086105–4.
- (62) We use a slab which is 16 Å deep. We place the proton in its middle, i.e., approximately 8 Å from the surface, deep enough so that the material already behaves as in the bulk phase.³⁴
- (63) In ref 11, the authors define the endothermicity for bulk dissolution differently. For this reason, their value is compared to our total dissolution energy 2.17 eV; 1.50 eV from absorption to subsurface; and 0.67 eV for the proton to go from subsurface to bulk, where both contributions are endothermic.
- (64) Huang, W.-F.; Chen, H.-T.; Lin, M. C. *J. Phys. Chem. C* **2009**, *113*, 20411–20420.
- (65) Hammer, B.; Wendt, S.; Besenbacher, F. *Top. Catal.* **2010**, *53*, 423–430.
- (66) Shannon, R. *Acta Crystallogr. A* **1976**, *32*, 751–767.
- (67) Diebold, U.; Li, S.-C.; Schmid, M. *Annu. Rev. Phys. Chem.* **2010**, *61*, 129–148.
- (68) Jiang, D. E.; Carter, E. A. *J. Phys. Chem. B* **2005**, *109*, 20469–20478.
- (69) Vineyard, G. *J. Phys. Chem. Solids* **1957**, *3*, 121–127.
- (70) Krishnamurthy, R.; Yoon, Y.; Srolovitz, D.; Car, R. *J. Am. Ceram. Soc.* **2004**, *87*, 1821–1830.
- (71) Kushima, A.; Yildiz, B. *ECS Trans.* **2009**, *25*, 1599.
- (72) Kushima, A.; Yildiz, B. *J. Mater. Chem.* **2010**, *20*, 4809–4819.
- (73) van Duin, A. C. T.; Merinov, B. V.; Jang, S. S.; Goddard, W. A., III *J. Phys. Chem. A* **2008**, *112*, 3133–3140.
- (74) Momma, K.; Izumi, F. *J. Appl. Crystallogr.* **2008**, *41*, 653–658.